Inorganic Chemistry

Article

pubs.acs.org/IC

# Substrate and Metal Control of Barrier Heights for Oxo Transfer to Mo and W Bis-dithiolene Sites

Adam L. Tenderholt,[†] Keith O. Hodgson,*[,†,‡] Britt Hedman,*[,‡] Richard H. Holm,*[,§] and Edward I. Solomon*[,†,‡]

[†]Department of Chemistry, Stanford University, Stanford, California 94305, United States

[‡]Stanford Synchrotron Radiation Lightsource, SLAC National Accelerator Laboratory, Stanford University, Menlo Park, California 94025, United States

[§]Department of Chemistry and Chemical Biology, Harvard University, Cambridge Massachusetts 02138, United States

S Supporting Information

**ABSTRACT:** Reaction coordinates for oxo transfer from the substrates $Me_3NO$, $Me_2SO$, and $Me_3PO$ to the biologically relevant Mo(IV) bis-dithiolene complex $[Mo(OMe)(mdt)_2]^-$ where mdt = 1,2-dimethyl-ethene-1,2-dithiolate(2-), and from $Me_2SO$ to the analogous W(IV) complex, have been calculated using density functional theory. In each case, the reaction first proceeds through a transition state (TS1) to an intermediate with substrate weakly bound, followed by a second transition state (TS2) around which breaking of the substrate X−O bond begins. By analyzing the energetic contributions to each barrier, it is shown that the nature of the substrate and metal determines which transition state controls the rate-determining step of the reaction.

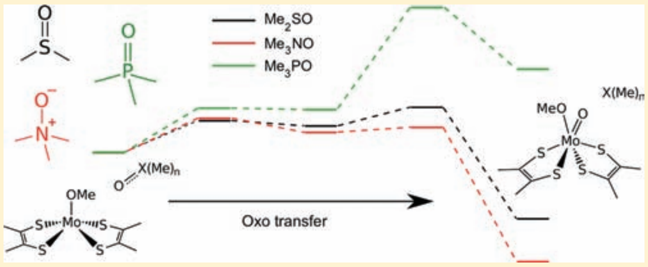

## 1. INTRODUCTION

Mononuclear molybdenum enzymes are present in all forms of life, ranging from archaea to mammals, and most catalyze oxo transfer reactions.[1,2] These enzymes are divided into three groups based upon the protein sequences and structures of the active sites: the DMSO reductase (DMSOr), sulfite oxidase, and xanthine oxidase families. Members of each family cycle between the Mo(IV) and Mo(VI) oxidation states and contain at least one pyranopterindithiolene cofactor. The Mo(IV) sites in the DMSO reductase family contain two pyranopterindithiolene ligands and a protein-derived ligand such as serine, cysteine, or selenocysteine, while the Mo(VI) site has an additional strong oxo ligand.[3,4]

The first structural models of the DMSOr active sites were molybdenum and tungsten bis-dithiolene complexes with a siloxyl ligand modeling the Mo−O bond to serine: $[M^{IV}(OSi)(bdt)_2]^-$ and $[M^{VI}O(OSi)(bdt)_2]^-$, where M = Mo or W, OSi = $[OSiPh_2{}^tBu]^-$, and bdt = benzene-1,2-dithiolate(2-).[5] The M(IV) des-oxo complexes exhibit slow oxo transfer, likely because of the steric bulk of the siloxyl ligand. A more functional set of complexes soon followed that incorporated a less bulky phenoxyl ligand instead of the siloxyl and a slightly different dithiolene ligand, 1,2-dimethyl-ethene-1,2-dithiolate-(2-) (mdt).[6] Kinetics parameters of oxo transfer to these and related M(IV) des-oxo complexes from a variety of substrates including $Me_3NO$ and $Me_2SO$ have been determined and showed that the reaction rate is substrate- and metal-dependent.[7−10]

In a previous study, we experimentally and computationally defined the electronic structure of $[Mo^{IV}(OSi)(bdt)_2]^-$ and $[Mo^{VI}O(OSi)(bdt)_2]^-$ using sulfur K-edge X-ray absorption spectroscopy and density functional theory (DFT).[11] Those results were then used to calculate a reaction coordinate for oxo transfer from $Me_2SO$ to the analogous $[Mo^{IV}(OMe)(mdt)_2]^-$ complex[12] to gain insight into the factors that control the energetics of transition states, the nature of oxo transfer, and the role of the dithiolene ligand. In particular, the oxo transfer reaction was found to be a concerted process where two electrons are transferred from the molybdenum complex to the S−O $\sigma^*$ orbital concurrently with electron transfer from the oxygen to sulfur, and the dithiolene was found to stabilize a singlet Mo(IV) complex which allows for more efficient oxo transfer than a triplet Mo(IV) complex. In this study, these experimentally supported calculations are extended to evaluate the trends in reactivity with other substrates (i.e., $Me_3NO$ and $Me_3PO$) and tungsten substitution to further validate the reaction coordinate presented in ref 11 and determine the contributions of each transition state to the rate-determining step.

## 2. COMPUTATIONAL DETAILS

Density functional theory calculations were peformed using the Gaussian 03 package[13] or, for relativistic calculations, ORCA.[14] The hybrid functional B3LYP,[15] which has Becke GGA exchange[16]

**Received:** September 19, 2011
**Published:** February 28, 2012

dx.doi.org/10.1021/ic2020397 | *Inorg. Chem.* 2012, 51, 3436−3442

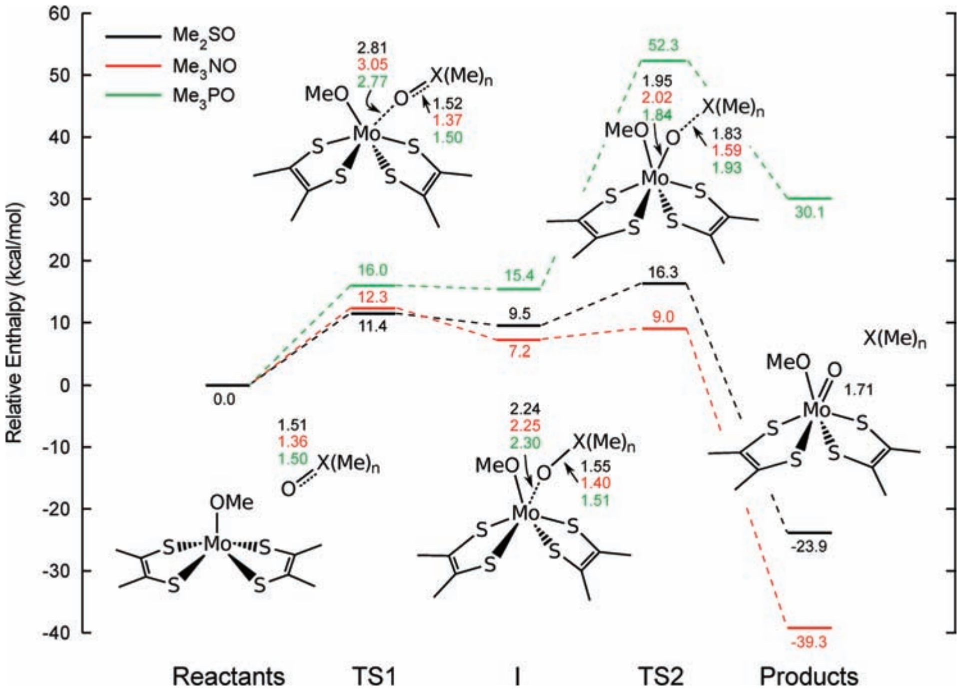

**Figure 1.** Reaction coordinate for oxo transfer from $Me_2SO$ (black), $Me_3NO$ (red), $Me_3PO$ (green) to $[Mo(OMe)(mdt)_2]^-$. Note that enthalpies are used instead of free energies because calculated entropies are in poor agreement with experiment (see Discussion), likely because the calculated values do not properly reflect the conformational space available to incoming substrate. The calculated enthalpies, however, are in good agreement with experimental data.

modified to include Hartree−Fock mixing with Lee, Yang, and Parr correlation,[17,18] was used as it was shown previously to give accurate electronic structure descriptions of the reactant $[Mo(OMe)(mdt)_2]^-$ and product $[MoO(OMe)(mdt)_2]^-$ complexes.[11] For Gaussian calculations, the SDD basis set,[19] which is triple-$\zeta$ quality with an effective core potential (ECP), and further augmented with additional polarization functions,[20] was used for the molybdenum and tungsten atoms. The 6-311G(d) basis set was used for oxygen, nitrogen, sulfur, and phosphorus atoms, and the 6-31G(d) basis set was used for the carbon and hydrogen atoms. For ORCA calculaions, the SARC-DKH basis set[21] was used for tungsten while the Ahlrichs-TZV basis sets[22] supplemented with auxiliary basis sets from the Tubomole library[23,24] were used for the molybdenum, sulfur, oxygen, carbon, and hydrogen atoms. Relativistic effects were included using a DKH Hamiltonian.[25]

Geometry optimizations and frequency calculations were performed without solvent corrections. Only the closed-shell singlet reaction coordinates are considered in this study because it was previously found[11] that reaction coordinates involving triplet reactants are unfavorable by ~10 kcal/mol and attempts to find open-shell singlet states (including at the oxo-transfer transition state) converged to a closed-shell wave function. No imaginary modes were found for stationary states and transition state structures were confirmed to have a single imaginary mode corresponding to the reaction coordinate. Single point calculations were performed using the polarizable continuum model (PCM)[26] using the default parameters for acetonitrile. The differences in nonelectrostatic contributions at each state for the reaction coordinates are small (<2−2.3 kcal/mol, Supporting Information). Attempts to find a reaction coordinate containing an explicit solvent molecule (i.e., seven-membered transition states) were unsuccessful. Indeed, these are unlikely because the solvent-bound $[Mo(OMe)(mdt)_2]^-$ complex is significantly higher in energy ($\Delta H$ = 14.0 and $\Delta G$ = 25.1 kcal/mol) than the isolated complex, indicating that the population of solvent-bound complex in solution is negligible. Furthermore, the enthalpy of the solvent-bound complex is larger than the enthalpies of the DMSO- and TMNO-bound intermediates (9.5 and 7.2 kcal/mol, respectively), and slightly smaller than the enthalpy of the TMPO-bound intermediate (15.4 kcal/mol). These results indicate that the substrate-bound intermediates form from free complex.

The three energetic contributions to each state along the reaction coordinate (i.e., distortion of the metal-dithiolene complex and the substrate, and the interaction between these two) were determined as follows. The distortion energies are the relative energies of either the metal-dithiolene complex or substrate at their distorted structure along the reaction coordinate (i.e., TS1, I, or TS2) compared with their fully optimized reactant structures. The interaction energy is the difference between the energy of the combined metal-dithiolene-substrate complex and the sum of the isolated metal-dithiolene complex and substrate energies at their distorted structures.

Condensed Fukui functions[27] were calculated using atomic Mulliken[28] charges. Molecular orbital compositions (using Mulliken population analysis) and Mayer bond orders[29,30] were calculated using QMForge,[31] which is built upon the cclib library.[32]

As suggested by a reviewer, we also explored the possibility of a reaction involving loss of the alkyl ligand (i.e., $MeO^-$, see Supporting Information). The most energetically favorable reaction yields $[Mo^VO(mdt)_2]^-$ and $MeOSMe_2$ ($\Delta E$ = 0.3 kcal/mol), which is ~29 kcal/mol higher in energy than the reaction yielding $[Mo^{VI}O(OMe)(mdt)_2]^-$ and $Me_2SO$, indicating that it is not a relevant reaction pathway.

## 3. RESULTS

**3.1. Trends of Oxo Transfer Reaction Coordinates.** The DFT-calculated reaction coordinates for oxo transfer from a variety of X−O substrates to $[Mo(OMe)(mdt)_2]^-$ are presented in Figure 1. As was shown previously,[11] oxo transfer from $Me_2SO$ (black) initially proceeds through a transition state (TS1) with a $Mo-O(SMe_2)$ distance of 2.81 Å (Mo−O). The $Me_2SO$ S−O bond has lengthened slightly from 1.51 Å to 1.52 Å. This transition state is followed by an intermediate (I) characterized by a weakly bound DMSO with a $(Me_2S)O-Mo$ distance of 2.24 Å and another slight elongation (0.03 Å) of the S−O bond to 1.55 Å indicating that the S−O bond is mostly

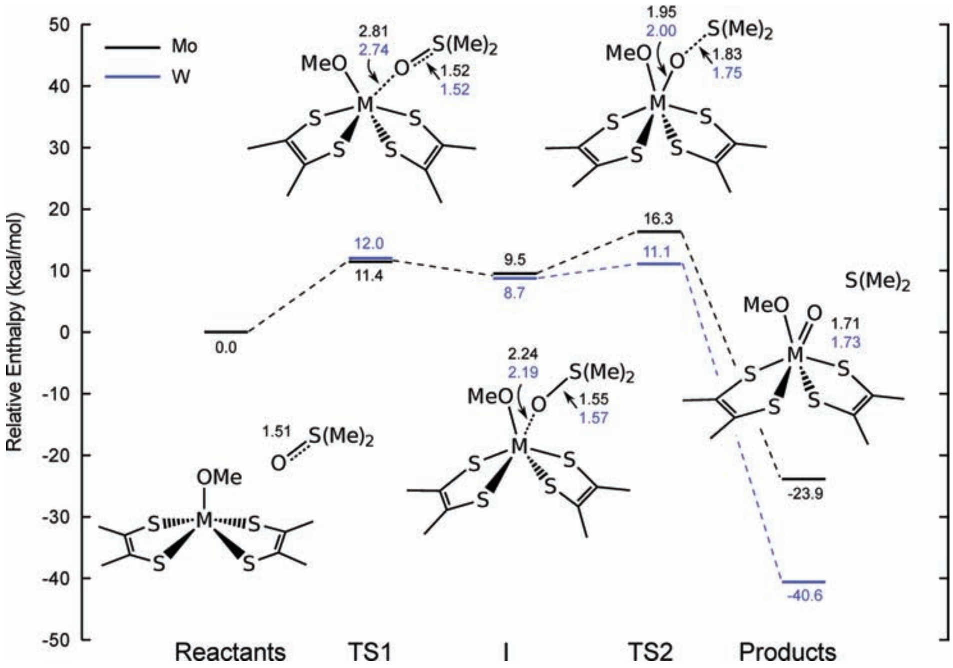

**Figure 2.** Reaction coordinate for oxo transfer from $Me_2SO$ to $[Mo(OMe)(mdt)_2]^-$ (black) and $[W(OMe)(mdt)_2]^-$ (blue).

intact. The reaction then proceeds through a second transition state (TS2) which is the largest barrier of the reaction ($\Delta H^\ddagger$ = 16.3 kcal/mol), in agreement with the experimental enthalpy of activation (14.9 kcal/mol) for oxo transfer to $[Mo(OPh)(mdt)_2]^-$.[6] The salient features of TS2 are a $(Me_2S)O-Mo$ distance of 1.95 Å and a S−O bond that is significantly lengthened to 1.83 Å. Finally, the product Mo(VI)=O bis-dithiolene complexes has a Mo=O bond length of 1.71 Å. These structural changes along the reaction coordinate are consistent with S−O bond breaking primarily occurring around TS2.

The reaction coordinate for oxo transfer from $Me_3NO$ (red in Figure 1) to $[Mo(OMe)(mdt)_2]^-$ is similar to that of $Me_2SO$. The first transition state (TS1) is characterized by a $(Me_3N)O-Mo$ distance of 3.05 Å and the N−O bond that has been elongated from 1.36 Å found in free $Me_3NO$ to 1.37 Å. This state is the largest barrier of the reaction coordinate, in contrast to that for the $Me_2SO$ reaction, with a calculated $\Delta H^\ddagger$ = 12.3 kcal/mol which is in modest agreement with the experimental enthalpy of activation (8.1 kcal/mol) for oxo transfer to $[Mo(OPh)(mdt)_2]1^-$.[8] The reaction then continues through an intermediate (I) with a $(Me_3N)O-Mo$ distance of 2.25 Å and a N−O distance of 1.40 Å (a limited 0.03 Å increase). Note that in a recent study, this stable intermediate structure was not found.[33] The second transition state (TS2) again is associated with X−O bond breaking, with the N−O bond being significantly lengthened by 0.19 Å to 1.59 Å and a decrease of the $(Me_3N)O-Mo$ distance to 2.02 Å. Finally, note that $\Delta H_{rxn} = -39.3$ kcal/mol, which is 15.4 kcal/mol more exothermic than the products of the reaction with DMSO and consistent with the differences in experimental X−O bond enthalpies for $Me_2SO$ (−27.1 kcal/mol) and $Me_3NO$ (−11 kcal/mol).[34] Thus, the reaction coordinate of oxo transfer from $Me_3NO$ to $[Mo(OMe)(mdt)_2]^-$ is similar to that of $Me_2SO$, except with TS1 being the largest barrier.

Oxo transfer from $Me_3PO$ to $[Mo(OMe)(mdt)_2]^-$ (green in Figure 1) proceeds along a reaction coordinate similar to that of $Me_2SO$ and $Me_3NO$. The first transition state (TS1) has a $(Me_3P)O-Mo$ distance of 2.77 Å and a P−O bond length of 1.50 Å (similar to free $Me_3PO$). In going to the intermediate (I), the $(Me_3P)O-Mo$ distance decreases to 2.30 Å and the P−O bond length increases slightly to 1.51 Å. The second transition state (TS2) is characterized by a significantly longer P−O bond (1.93 Å) while the $(Me_3P)O-Mo$ distance has decreased to 1.84 Å. This is the largest barrier along the coordinate, with an enthalpy of activation ($\Delta H^\ddagger$ = 52.3 kcal/mol) consistent with the lack of oxo transfer from $Me_3PO$ to $[Mo(OMe)(mdt)_2]^-$. Note that reverse oxo transfer has been observed from several Mo(VI) bis-oxo sites to a variety of tertiary phosphines ($R_3P$).[35−37] Finally, the products of this coordinate are 54 kcal/mol higher in energy than for oxo transfer from $Me_2SO$, in agreement with differences in experimental gas phase bond enthalpies between $Me_2SO$ (−27.1 kcal/mol) and $Me_3PO$ (−79.7 kcal/mol).[34]

Figure 2 shows the reaction coordinate of oxo transfer from $Me_2SO$ to $W(OMe)(mdt)_2]^-$ (blue) relative to the Mo analogue (black), which is similar to the other reactions above. Oxo transfer first proceeds through a transition state (TS1) with a $W-O(SMe_2)$ distance of 2.74 Å and a slightly elongated S−O bond (1.52 Å). At the intermediate (I), the $W-O(SMe_2)$ distance has decreased to 2.19 Å and the S−O bond length has increased to 1.57 Å. Both of these structural parameters suggest that the intermediate occurs later on the reaction coordinate compared with the Mo-$Me_2SO$ intermediate. As with the other reactions, in going to the second transition state (TS2), the substrate X−O (i.e., S−O) bond length has increased significantly to 1.75 Å indicating a substantial weakening of the S−O bond. The $W-O(SMe_2)$ distance has also decreased to 2.00 Å. Of particular note is that the enthalpy of TS2 is 11.1 kcal/mol, which is 5.2 kcal/mol lower in energy than for the reaction with Mo, and is not significantly different than the enthalpy of TS1 (12.0 kcal/mol). This energetic difference, along with the structural parameters, suggest that TS2 occurs earlier along the reaction coordinate compared with the Mo-$Me_2SO$ reaction, indicating that the W-$Me_2SO$ reaction is more facile in agreement with experimental kinetic studies ($k_W = 3.9 \times 10^{-5}$ $M^{-1}$ $s^{-1}$ vs $k_{Mo} = 1.3 \times 10^{-5}$ $M^{-1}$ $s^{-1}$). We have previously proposed that such differences in reactivity are due to larger relativistic effects in tungsten,[38] which would facilitate electron transfer from an occupied metal-based orbital to the S−O $\sigma^*$ orbital.[11] Indeed, calculations using all-electron basis sets without and with relativistic effects show that inclusion of relativistic effects destabilizes the redox-active tungsten orbital by ~0.2 eV in both the free $[W(OMe)(mdt)_2]^-$ and the DMSO-bound intermediate (Supporting Information), and thus, the energy of TS2 is expected to be about ~4.5 kcal/mol lower in energy.[39] Finally, the reaction proceeds to the W(VI) oxo product $[WO(OMe)(mdt)_2]^-$ and $Me_2S$. The calculated energy difference between the Mo and W products (16.7 kcal/mol) is less than seen for the experimental M−O bond strengths of complexes such as $MOCl_4$ (~26 kcal/mol);[40] however, this difference is primarily due to differences in ligands (i.e., dithiolenes vs chlorides) and their covalent interactions with the metal center.[41]

**3.2. Energetic Contributions to Oxo Transfer Reaction Coordinate.** Additional insight into the substrate (and metal) control of reaction barrier heights can be gained by considering the three energetic contributions to each state along the reaction coordinate (Figure 3a): (1) the distortion of the metal complex to accommodate incoming substrate and going from the five-coordinate reactant to six-coordinate product (red), (2) the lengthening and breaking of the substrate X−O bond (green), and (3) the interaction between these two fragments (blue).

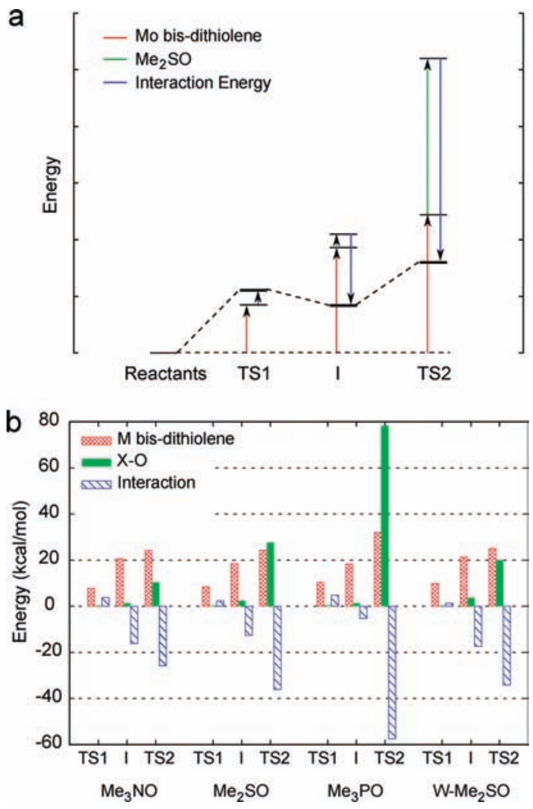

**Figure 3.** (a) Three energetic contributions to each state of the reaction coordinate, that is, the distortions of the $[M(OMe)(mdt)_2]^-$(M = Mo, W) complex (red), substrate (green), and their interaction (blue), and (b) these contributions for the oxo transfer reaction coordinates in Figures 1 and 2.

There are some noteworthy trends for each of the reaction coordinates in Figures 1 and 2. First, the primary energetic contribution to TS1 is the distortion of the M−OMe bond of the metal complex (red in Figure 3) away from the axial position to accommodate the incoming substrate. There is no signficant contribution from the distortion of the substrate (green in Figure 3) such as lengthening of the X−O bond, and the interaction between the substrate and the metal complex is minor (blue in Figure 3). Next, in going to the intermediate, the energy of the metal complex increases to further accommodate the substrate and the interaction between the metal complex and substrate has increased (i.e., becomes more negative, indicating a more favorable interaction). Finally, at TS2, the major energetic contributions are the significant lengthening of the X−O bond (see Figures 1 and 2) and the signficant interaction between the metal complex and substrate.

The fundamental differences in the reaction coordinates in Figure 1 can be understood by considering the energetic contributions in Figure 3b. At TS1, the enthalpies of each reaction are similar, and there are no obvious differences in the three energetic contributions. However, the enthalpy at TS1 for the reaction with $Me_3PO$ is slightly larger (16.0 kcal/mol) than for the reactions with $Me_2SO$ and $Me_3NO$ (11.4 and 12.3 kcal/mol, respectively). This is reasonable since the steric demands of $Me_3PO$ are larger than both $Me_2SO$ (three vs two methyl groups) and $Me_3NO$ (smaller cone angle for amines than phosphines). In going to I, there are more significant differences between the three reactions. The magnitude of the interaction energies decrease (i.e., become less favorable) in the order $Me_3NO > Me_2SO > Me_3PO$. Some of this reflects the Mo−O distances (2.25 vs 2.30 Å for $Me_2SO$ and $Me_3PO$, respectively), while the nature of the substrate has some influence. Specifically, the condensed Fukui functions show that $Me_3NO$ ($f_O^- = 0.56$) is a better electrophile than either $Me_2SO$ ($f_O^- = 0.37$) or $Me_3PO$ ($f_O^- = 0.36$). Finally, at TS2, the differences among the substrates are the largest. The energy required to lengthen the X−O bond to the TS2 geometry increases in the order $Me_3NO < Me_2SO < Me_3PO$, reflecting the increases in X−O distances in going from I to TS2: 0.19 Å, 0.28 Å, and 0.42 Å for $Me_3NO$, $Me_2SO$, and $Me_3PO$, respectively. A similar trend is observed for the magnitude of interaction energies (i.e., $Me_3NO < Me_2SO < Me_3PO$) which reflects the $Mo-O(XMe_n)$ distances, with larger distances (2.02 Å, 1.95 Å, and 1.84 Å for $Me_3NO$, $Me_2SO$, $Me_3PO$, respectively) leading to less spatial overlap between fragment molecular orbitals, and thus, smaller interaction energies. Note that these trends mirror that of the substrate X−O bond strengths (i.e., $Me_3NO < Me_2SO < Me_3PO$) indicating that the nature of the substrate controls the height of the oxo transfer barrier TS2, and thus, the inherent features of the reaction coordinate (i.e., whether the rate-limiting step is TS1 or TS2).

A similar analysis provides insight into influence of tungsten substitution. The enthalpies and structural parameters for oxo transfer to $[M(OMe)(mdt)_2]^-$ (M = Mo, W) complexes in Figure 2 are very similar for TS1 and I, although the slightly shorter $M-O(SMe_2)$ and longer S−O distances again suggest that these states occur "later" along the reaction coordinate for tungsten. This is also reflected in the energy analysis in Figure 3b, that is, the magnitudes of the substrate distortion and interaction energies are larger for tungsten at I (−17.4 kcal/mol vs −12.6 kcal/mol for Mo). The major differences between molybdenum and tungsten appear at TS2. In going to W, the magnitudes of the substrate distortion and interaction energies decrease (i.e., 19.9 and 34.3 kcal/mol, respectively, versus 27.6 and 36.1 kcal/mol for Mo). This is also reflected by a shorter S–O bond (1.75 Å for W vs 1.83 Å for Mo) and greater M–O($SMe_2$) distances (2.00 Å vs 1.95 Å for W and Mo, respectively). These results suggest that for tungsten, the transition state for oxo transfer (TS2) is "earlier" along the reaction coordinate.

## 4. DISCUSSION

The substrate- and metal-control of the reaction coordinate originates from the mechanism of oxo transfer. As we described previously,[11] oxo transfer occurs as two electrons are transferred from a filled M $d_{z^2}$ orbital (based on the symmetry of the intermediate) into the substrate X–O $\sigma^*$ orbital (Figure 4). This process is facilitated by the lengthening of the X–O bond which stabilizes the X–O $\sigma^*$ orbital relative to the metal orbital while simultatenously leading to an increase in the oxygen character of this orbital. Both of these changes increase the mixing coefficients between the X–O $\sigma^*$ and M $d_{z^2}$ orbitals. Thus, the energy and oxygen character of the X–O $\sigma^*$ orbital have to reach certain thresholds before there is enough bonding (i.e., interaction energy) between the metal complex and the substrate to offset the increase in energy for distorting the X–O bond, and thus, overcome the barrier associated with oxo transer. Note that for oxo transfer from $Me_2SO$ to the W complex, the W $d_{z^2}$ orbital is destabilized because of relativistic effects (Supporting Information), and thus, has better bonding with the incoming $Me_2SO$ compared with the Mo complex for a given S–O bond length; TS2 will, therefore, occur "earlier" on the W reaction coordinate.

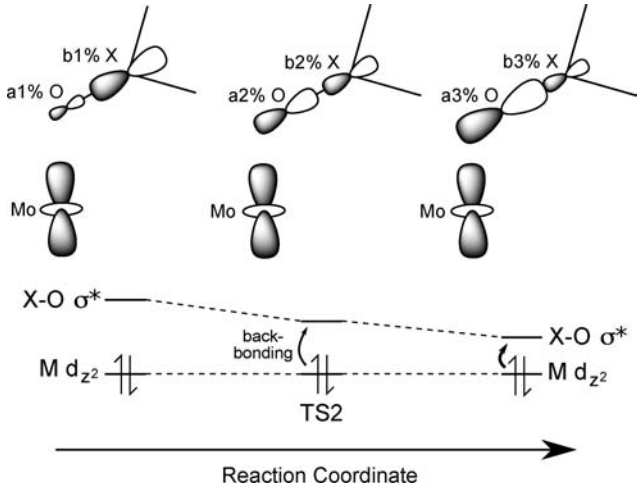

**Figure 4.** Oxo transfer occurs as two electrons are transferred from a filled metal-based orbital to the substrate X–O $\sigma^*$ orbital. Along the reaction coordinate, the X–O bond is lengthened which stabilizes the X–O $\sigma^*$ orbital relative to the metal orbital and increases its O character.

Figure 5 shows the energies and oxygen character of the X–O $\sigma^*$ orbitals as a function of X–O bond length increase around TS2; the fraction of the remaining X–O bonds are also listed. Note that approximate bond length increases associated with TS2 for each reaction coordinate are highlighted: ~0.2 Å ($Me_3NO$), ~0.3 Å ($Me_2SO$), and ~0.4 Å ($Me_3PO$). As the bonds are lengthened, these orbitals are stabilized, and their oxygen character increases. Despite the energy of the N–O $\sigma^*$ orbital (red) being higher than this orbital for the other substrates at all distances, it has significant oxygen character (41%) at a modest N–O bond length corresponding to its TS2 (~0.2 Å); this corresponds to 0.84 of the N–O bond remaining intact. Interestingly, the oxygen character increases to nearly this amount for $Me_2SO$ (38%) and $Me_3PO$ (34%) at the bond length distortions associated with their transition states (~0.3 Å and ~0.4 Å, respectively). Similarly, the fraction of the remaining S–O and P–O bonds at their transition states (0.85 and 0.86 for $Me_2SO$ and $Me_3PO$, respectively) approaches that seen for the N–O bond in $Me_3NO$ (0.84). These results suggest that the amount of oxygen character in the X–O $\sigma^*$ orbital (as manifested in the X–O bond strength) is the dominant factor controlling the barrier height of TS2, while the energy of this orbital has less effect.

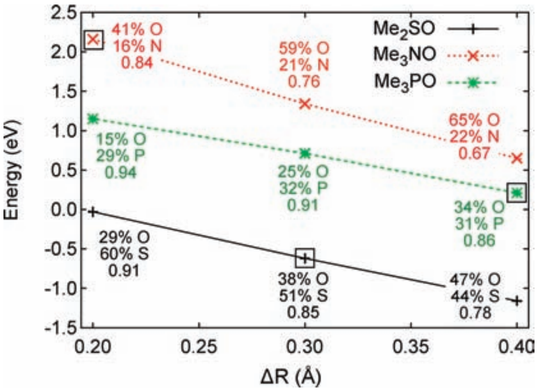

**Figure 5.** Energies of the X–O $\sigma^*$ orbitals as a function of increase in X–O bond length for free substrate. At each structure, the O p and X p orbital composition is listed along with the fraction of the remaining X–O bond based on Mayer bond order. Note that the distortions marked approximately correspond to the TS2 structures: ~0.2 Å ($Me_3NO$), ~0.3 Å ($Me_2SO$), and ~0.4 Å ($Me_3PO$).

There have been discussions as to whether TS1 or TS2 is the rate-limiting step based on experimental and computation results. Experimental kinetics data indicate that while increases in reaction rates follow the same trend as X–O bond strengths, which suggests TS2 is the rate-limiting step, reaction rates sometimes correlate better with substrate $pK_a$'s and proton affinities suggesting that TS1 is the rate-limiting step. Furthermore, calculations for oxo transfer from S–O substrates such as $Me_2SO$ consistently show that TS2 is the rate-limiting step.[42−44] We previously proposed[11] a qualitative model that reconciles the experimental and computational results based on an understanding of the factors that control the heights of the barriers for oxo transfer from $Me_2SO$ to $[Mo(OMe)(mdt)_2]^-$ (Figure 3). Now, with the results in Figures 1 and 2, the degree of rate control for each transition state can be evaluated more quantitatively.

The calculated degree of rate control ($\chi_i$) provides a quantitative measure of how much a transition state contributes to the rate of a reaction.[45] Figure 6 shows the $\chi_i$'s for TS1 and TS2 using the calculated enthalpies of activation from Figures 1 and 2 (Supporting Information). Note that these values are plotted as a function of the difference in entropies of activation since DFT optimizations do not fully sample the conformational space surrounding transition states, and thus, calculated $\Delta S^‡$'s are unreliable. Indeed, this is reflected in the poor agreement between experimental ($\Delta S^‡ = -19$ to $-39$ cal/(mol K), Table 1) and computational values ($\Delta S^‡ \approx -45$ cal/(mol K), Supporting Information). For the reaction with $Me_2SO$

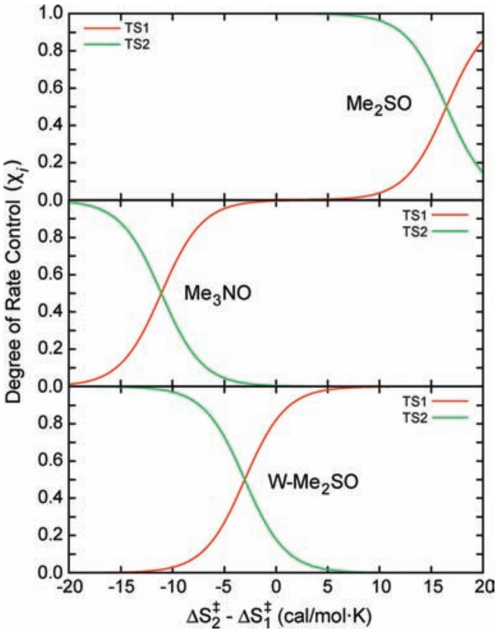

**Figure 6.** Calculated degree of rate-control for each transition state along the oxo-transfer reaction coordinates in Figures 1 and 2, as a function of the differences in the entropies of activation.

**Table 1. Comparison of Experimental Enthalpies and Entropies of Activation for Oxo Transfer to M(IV) Bis-dithiolene Complexes**[a]

| complex | substrate | $\Delta H^\ddagger$ (kcal/mol) | $\Delta S^\ddagger$ (cal/(mol K)) | ref. |
|---|---|---|---|---|
| $[W(O^iPr)(mdt)_2]^-$ | $Me_3NO$ | 12(5) | −19(3) | 9 |
| $[Mo(OPh)(mdt)_2]^-$ | $(PhCH_2)_3NO$ | 9.5(1) | −21(1) | 8 |
| | $Me_3NO$ | 8.1(6) | −21(2) | |
| $[W(OC_6H_4-pNH_2)(mdt)_2]^-$ | $(CH_2)_4SO$ | 15(1) | −24(4) | 9 |
| $[W(OPh)(mdt)_2]^-$ | $C_5H_5NO$ | 9.9(9) | −27(4) | 9 |
| | $Me_2SO$ | 14.4(2) | −30(1) | |
| $[Mo(OC_6F_5)(mdt)_2]^-$ | $(CH_2)_4SO$[b] | 11.8(3) | −30(5) | 8 |
| $[W(OPh)(mdt)_2]^-$ | $(CH_2)_4SO$ | 11.6(4) | −33(1) | 9 |
| $[Mo(OPh)(mdt)_2]^-$ | $Me_2SO$ | 14.8(5) | −36(1) | 6 |
| | $(CH_2)_4SO$ | 10.1(4) | −39(1) | |

[a] $CH_3CN$. [b] THF.

(top panel), the second transition state is completely rate-limiting (i.e., $\chi_{TS2} = 1.0$) for $\Delta S_{TS2}{}^\ddagger - \Delta S_{TS1}{}^\ddagger < \sim 8$ cal/(mol K). Since the number of available conformations are likely to be smaller for TS2 (i.e., less conformational flexibility once Mo−O bonding is significant), $\Delta S_{TS2}{}^\ddagger < \Delta S_{TS1}{}^\ddagger$. Therefore, TS2 is the rate-limiting step for oxo-transfer from $Me_2SO$ to Mo(IV) des-oxo sites. In constrast, the rate of oxo transfer from $Me_3NO$ (middle panel) is primarily controlled by TS1 for $\Delta S_{TS2}{}^\ddagger - \Delta S_{TS1}{}^\ddagger > \sim -10$ cal/(mol K). Since TS2 occurs early for this reaction (based on bond lengths and orbital character), the entropies of activation for TS1 and TS2 are probably similar, and thus, the rate of oxo-transfer from $Me_3NO$ to Mo(IV) des-oxo sites is likely to be controlled by TS1. Finally, for oxo transfer from $Me_2SO$ to $[W(OMe)(mdt)_2]^-$, the rate control is highly dependent on the difference in entropies of activation; both transition states have significant control ($\chi_i > 0.1$) for reasonable values ($-10 < \Delta S_{TS2}{}^\ddagger - \Delta S_{TS1}{}^\ddagger < 0$). Therefore, the nature of the rate-limiting step is very system-specific for oxo transfer from S−O substrates to W(IV) des-oxo sites.

Additional evidence for the substrate control of the rate-limiting step is suggested by the experimental entropies of activation. These values for various oxo transfer reactions are listed in Table 1, sorted by increasingly negative $\Delta S^\ddagger$. Here, some interesting patterns emerge. Reactions with $R_3NO$ substrates have $\Delta S^\ddagger$'s ranging from −19 to −21 cal/(mol K), while those with S−O substrates (except for one reaction with a W complex) are more negative ($\Delta S^\ddagger = -30$ to −39 cal/(mol K)). The reaction with $C_5H_5NO$ is unique, likely because it has an $sp^2$-hydridized N in contrast to the $sp^3$-hybridized N found in the $R_3NO$ substrates. Also, note that the activation entropies for reactions involving W complexes are smaller than their Mo analogues (i.e., $|\Delta S^\ddagger(W)| < |\Delta S^\ddagger(Mo)|$). These observations, coupled with the reaction coordinates and the analyses above, suggest two general rules about oxo transfer reactions to M(IV) bis-dithiolene complexes (M = Mo, W). First, reactions involving S−O substrates will have TS2 as the rate-limiting step with large, negative entropies of activation (ca. −30 cal/(mol K)) because of the limited conformations at TS2. Second, for reactions involving N−O substrates, the rate-limiting step will be TS1, and the entropies of activation will be less negative (ca. −20 cal/(mol K)) since there is more conformational flexibility for the incoming substrate at TS1.

## 5. CONCLUSION

Reaction coordinates have been calculated for oxo transfer from substrates with varying X−O bond strengths (i.e., $Me_3NO$, $Me_2SO$, and $Me_3PO$) to the biologically relevant Mo(IV) bis-dithiolene complex $[Mo(OMe)(mdt)_2]^-$, as well as for oxo transfer from $Me_2SO$ to the analogous W(IV) complex. Each reaction coordinate proceeds through a transition state (TS1) with little X−O bond lengthening followed by a substrate-bound intermediate. Oxo transfer primarily occurs around the second transition state (TS2), as seen by both geometric parameters and the energetic contributions to this state. These results indicate that the amount of oxygen character in the X−O $\sigma^*$ orbital dramatically affects the amount of lengthening of the X−O bond required to reach TS2. This distortion is the primary contribution to the energy of TS2. Additionally, replacing Mo by W also lowers the energy of TS2 for oxo transfer from $Me_2SO$ to the metal bis-dithiolene complex because of the larger relativistic effects in W compared to Mo, which destabilize the redox active molecular orbital.[38] Such a destabilization results in a decreased energetic separation between the frontier molecular orbitals, and thus, a smaller lengthening of the S−O bond is required before electron transfer to the substrate begins. Since TS1 is less sensitive to the nature of the substrate, variation in TS2 because of differences in X−O bond strength determines which transition state controls the overall rate of the reaction. Therefore, the nature of the rate-limiting step (i.e., whether it involves oxo transfer or not) is substrate- and metal-dependent.

## ■ ASSOCIATED CONTENT

### Ⓢ Supporting Information

Derivation of the degrees of rate control ($\chi_i$); thermodynamic values for the reaction coordinates; energetics of alternative reaction pathways; contributions of relativistic effects; non-electrostatic energy contributions; complete citation for reference 13; Cartesian coordinates of the reactants, products, transition states, and intermediates. This material is available free of charge via the Internet at http://pubs.acs.org.

## AUTHOR INFORMATION

### Corresponding Author

*E-mail: hodgson@ssrl.slac.stanford.edu (K.O.H.), hedman@ssrl.slac.stanford.edu (B.H.), holm@chemistry.harvard.edu (R.H.H.), edward.solomon@stanford.edu (E.I.S.).

### Notes

The authors declare no competing financial interest.

## ACKNOWLEDGMENTS

This work was supported by NSF CHE 0948211 (E.I.S.), NIH RR-001209 (K.O.H.), NSF CHE 0547734 and CHE 0846397 (R.H.H.). A.L.T. would like to thank the Department of Chemistry, University of Washington, for providing some computational resources. This publication was partly made possible by Grant Number 5 P41 RR001209 from the National Center for Research Resources (NCRR), a component of the National Institutes of Health (NIH). Its contents are solely the responsibility of the authors and do not necessarily represent the official view of NCRR or NIH.

## REFERENCES

(1) Hille, R. *Chem. Rev.* **1996**, *96*, 2757−2816.

(2) Hille, R. *Trends Biochem. Sci.* **2002**, *27*, 360−367.

(3) George, G. N.; Hilton, J.; Temple, C.; Prince, R. C.; Rajagopalan, K. V. *J. Am. Chem. Soc.* **1999**, *121*, 1256−1266.

(4) Romão, M. *Dalton Trans.* **2009**, *2009*, 4053−4068.

(5) Donahue, J. P.; Lorber, C.; Nordlander, E.; Holm, R. H. *J. Am. Chem. Soc.* **1998**, *120*, 3259−3260.

(6) Lim, B. S.; Sung, K.-M.; Holm, R. H. *J. Am. Chem. Soc.* **2000**, *122*, 7410−7411.

(7) Enemark, J. H.; Cooney, J. J. A.; Wang, J.-J.; Holm, R. H. *Chem. Rev.* **2004**, *104*, 1175−1200.

(8) Lim, B. S.; Holm, R. H. *J. Am. Chem. Soc.* **2001**, *123*, 1920−1930.

(9) Sung, K.-M.; Holm, R. H. *J. Am. Chem. Soc.* **2001**, *123*, 1931−1943.

(10) Sung, K.-M.; Holm, R. H. *J. Am. Chem. Soc.* **2002**, *124*, 4312−4320.

(11) Tenderholt, A. L.; Wang, J.-J.; Szilagyi, R. K.; Holm, R. H.; Hodgson, K. O.; Hedman, B.; Solomon, E. I. *J. Am. Chem. Soc.* **2010**, *132*, 8359−8371.

(12) The $[M^{IV}(OMe)(mdt)_2]^-$ (M = Mo, W) complexes are known and undergo oxygen atom transfer: Wang, J.-J.; Tessier, C.; Holm, R. H. *Inorg. Chem.* **2006**, *45*, 2979−2988.

(13) Frisch, M. J.; et al. *Gaussian 03*, revisions C.01 and E.01; Gaussian, Inc.: Wallingford, CT, 2004.

(14) Neese, F. *ORCA: An ab initio, DFT, and semiempirical electronic structure package*, Version 2.6 revision 35; Universität Bonn: Bonn, Germany, 2008.

(15) Becke, A. D. *J. Chem. Phys.* **1993**, *98*, 5648−5652.

(16) Becke, A. D. *Phys. Rev. A* **1988**, *83*, 3098−3100.

(17) Lee, C.; Yang, W.; Parr, R. G. *Phys. Rev. B* **1988**, *37*, 785−789.

(18) Miehlich, B.; Savin, A.; Stoll, H.; Preuss, H. *Chem. Phys. Lett.* **1989**, *157*, 200−206.

(19) Andrae, D.; Häußermann, U.; Dolg, M.; Stoll, H.; Preuß, H. *Theor. Chim. Acta* **1990**, *77*, 123−141.

(20) Ehlers, A.; Böhme, M.; Dapprich, S.; Gobbi, A.; Höllwarth, A.; Jonas, V.; Köhler, K.; Stegmann, R.; Veldkamp, A.; Frenking, G. *Chem. Phys. Lett.* **1993**, *208*, 111−114.

(21) Duboc, C.; Ganyushin, D.; Sivalingam, K.; Collomb, M.-N.; Neese, F. *J. Phys. Chem. A* **2010**, *114*, 10750−10758.

(22) Schäfer, A.; Horn, H.; Ahlrichs, R. *J. Chem. Phys.* **1992**, *97*, 2571−2577.

(23) Eichkorn, K.; Treutler, O.; Öhm, H.; Häser, M.; Ahlrichs, R. *Chem. Phys. Lett.* **1995**, *240*, 283−289.

(24) Eichkorn, K.; Weigend, F.; Treutler, O.; Ahlrichs, R. *Theor. Chem. Acc.* **1997**, *97*, 119−124.

(25) Jansen, G.; Hess, B. A. *Phys. Rev. A* **2011**, *39*, 6016−6017.

(26) Tomasi, J.; Mennucci, B.; Cammi, R. *Chem. Rev.* **2005**, *105*, 2999−3094.

(27) Yang, W.; Mortier, W. J. *J. Am. Chem. Soc.* **1986**, *108*, 5708−5711.

(28) Mulliken, R. *J. Chem. Phys.* **1955**, *23*, 1833−1840.

(29) Mayer, I. *Chem. Phys. Lett.* **1983**, *97*, 270−274.

(30) Bridgeman, A. J.; Cavigliasso, G.; Ireland, L. R.; Rothery, J. *J. Chem. Soc., Dalton Trans.* **2001**, 2095−2108.

(31) Tenderholt, A. L. *QMForge*, v. 2.1; Stanford University: Stanford, CA, 2007; http://qmforge.sourceforge.net.

(32) O'Boyle, N. M.; Tenderholt, A. L.; Langner, K. M. *J. Comput. Chem.* **2008**, *29*, 839−845.

(33) Mtei, R. P.; Lyashenko, G.; Stein, B.; Rubie, N.; Hille, R.; Kirk, M. L. *J. Am. Chem. Soc.* **2011**, *133*, 9762−9774.

(34) Lee, S.; Holm, R. H. *Inorg. Chim. Acta* **2008**, *361*, 1166−1176.

(35) Kail, B. W.; Pérez, L. M.; Zarić, S. D.; Millar, A. J.; Young, C. G.; Hall, M. B.; Basu, P. *Chem.—Eur. J.* **2006**, *12*, 7501−7509.

(36) Basu, P.; Nemykin, V. N.; Sengar, R. S. *Inorg. Chem.* **2009**, *48*, 6303−6313.

(37) Basu, P.; Kail, B. W.; Young, C. G. *Inorg. Chem.* **2010**, *49*, 4895−4900.

(38) Tenderholt, A. L.; Szilagyi, R. K.; Holm, R. H.; Hodgson, K. O.; Hedman, B.; Solomon, E. I. *J. Inorg. Biochem.* **2007**, *101*, 1594−1600.

(39) Note that the reaction coordinates are from calculations that use pseudopotentials, and thus, empirically include relativistic effects.

(40) Holm, R. H.; Donahue, J. P. *Polyhedron* **1993**, *12*, 571−589.

(41) The calculated differences in M−O bond strengths for $MoOCl_4$ vs $WOCl_4$ is 29.8 kcal/mol.

(42) Thapper, A.; Deeth, R. J.; Nordlander, E. *Inorg. Chem.* **2002**, *41*, 6695−6702.

(43) McNamara, J. P.; Mohr, M.; Wang, H.; Hillier, I. H. *Mol. Phys.* **2005**, *103*, 2465−2475.

(44) McNamara, J. P.; Hillier, I. H.; Bhachu, T. S.; Garner, C. D. *Dalton Trans.* **2005**, 3572−3579.

(45) Stegelmann, C.; Andreasen, A.; Campbell, C. T. *J. Am. Chem. Soc.* **2009**, *131*, 8077−8082.